EarthArXiv Coversheet

Title: Permafrost thaw subsidence, sea-level rise, and erosion are transforming Alaska's Arctic coastal zone

Authors:
Roger C. Creel
Roger.creel@whoi.edu, twitter: @rogercreel
Department of Physical Oceanography, Woods Hole Oceanographic Institution, Falmouth MA, USA

Julia Guimond
Department of Applied Ocean Physics and Engineering, Woods Hole Oceanographic Institution, Falmouth MA, USA

Benjamin Jones
Water and Environmental Research Center, University of Alaska, Fairbanks, Alaska, USA

David M. Nielsen
Max-Planck-Institut Für Meteorologie, Hamburg, Germany

Emily Bristol
Marine Science Institute, University of Texas at Austin, Texas, USA

Craig E. Tweedie
Department of Biological Sciences and the Environmental Science and Engineering Program, University of Texas as El Paso, Texas, USA

Pier Paul Overduin
Alfred Wegener Institute Helmholtz-Centre for Polar and Marine Research, Potsdam, Germany

Permafrost thaw subsidence, sea-level rise, and erosion are transforming Alaska's Arctic coastal zone

Roger Creel[a], **Julia Guimond**[b], **Benjamin Jones**[c], **David M. Nielsen**[d], **Emily Bristol**[e], **Craig E. Tweedie**[f], **and Pier Paul Overduin**[g]

This manuscript was compiled on May 10, 2024

Arctic shorelines are vulnerable to climate change impacts as sea level rises, permafrost thaws, storms intensify, and sea ice thins. Seventy-five years of aerial and satellite observations have established coastal erosion as an increasing Arctic hazard. However, other hazards at play—for instance, the cumulative impact that sea-level rise and permafrost thaw subsidence will have on permafrost shorelines—have received less attention, preventing assessments of these processes' impacts compared to and combined with coastal erosion. Alaska's Arctic Coastal Plain (ACP) is ideal for such assessments because of the high density observations of topography, coastal retreat rates, and permafrost characteristics, and importance to Indigenous communities. Here we produce the first 21st century projections of Arctic shoreline position that include erosion, permafrost subsidence, and sea-level rise. Focusing on the ACP, we merge 5 meter topography, satellite-derived coastal lake depth estimates, and empirical assessments of land subsidence due to permafrost thaw with projections of coastal erosion and sea-level rise for medium and high emissions scenarios from the Intergovernmental Panel on Climate Change's AR6 Report. We find that by 2100, erosion and inundation will together transform the ACP, causing 6-8x more land loss than coastal erosion alone causes and disturbing 8-11x more organic carbon. Without mitigating measures, by 2100 coastal change could damage 40-65% of infrastructure in present-day ACP coastal cities and towns, and 10-20% of oilfield infrastructure. Our findings highlight the risks that compounding climate hazards pose to coastal communities, and underscore the need for adaptive planning for communities within zones of 21st century land loss.

Permafrost thaw subsidence | Sea-level rise | Coastal erosion | Arctic | Climate hazards

Climatic warming is causing rapid changes to Arctic coastal regions. In the last four decades, Arctic temperatures have increased at four times the global mean (1). Rising temperatures are accompanied by a cascade of Earth system consequences: land ice is melting; sea ice extent is diminishing; open water periods are lengthening; sea level is rising; coastal erosion is intensifying; and frozen ground is thawing (2). Projections of climate evolution indicate that these trends will persist throughout the 21st century, and that the severity of the resulting impacts to coastal communities (3)—and the organic carbon (OC) and contaminants that get mobilized—will depend on the speed at which anthropogenic atmospheric greenhouse gas accumulation is reduced (4). In Alaska, and the Arctic as a whole, present-day climate changes are amplifying long-standing threats and introducing additional challenges to community adaptation—particularly coastal Indigenous communities. This heightened threat is in part because the compounding nature of these changes produces non-linear increases in coastal hazards (5).

Coastal erosion, subsidence from permafrost thaw (hereafter, permafrost subsidence), and sea-level rise have each individually received attention as important threats to Arctic landscapes. Thanks to repeat aerial surveys starting in middle of the 20th century (6), rates of Arctic coastal erosion are known to be among the highest in the world and to have accelerated throughout the last 80 years (7). Recent observations from a geographic spread of coastal monitoring sites provide a glimpse of how Arctic System changes are

Significance Statement

Climate warming is causing rapid coastal change in the Arctic. Permafrost thaw subsidence, sea-level rise, and erosion each threaten the Arctic nearshore. These agents of change have received unequal attention and their compound impact remains poorly understood. Alaska's Arctic Coastal Plain (ACP) is ideal for addressing this knowledge gap due to the region's relatively abundant observational data and importance to Indigenous communities, socioeconomics, and geopolitics. We present the first projections of 21st century ACP evolution that include subsidence, sea-level rise, and erosion. By 2100, 6-8x more land will be transformed by these compound effects than erosion alone would impact. Our findings underscore that coastal communities may need to consider a paradigm shift in how they adapt to 21st century Arctic coastal change.

Author affiliations: [a]Department of Physical Oceanography, Woods Hole Oceanographic Institution (WHOI), Falmouth MA, USA; [b]Department of Applied Ocean Physics and Engineering, WHOI, Falmouth MA, USA; [c]Water and Environmental Research Center, University of Alaska, Fairbanks, Alaska, USA; [d]Max-Planck-Institut Für Meteorologie, Hamburg, Germany; [e]Marine Science Institute, University of Texas at Austin, Texas, USA; [f]Department of Biological Sciences and the Environmental Science and Engineering Program, University of Texas as El Paso, Texas, USA; [g]Alfred Wegener Institute Helmholtz-Centre for Polar and Marine Research, Potsdam, Germany

Conceptualization: RC, JG, BJ; Methodology development: RC, BJ, JG; Data curation: RC, BJ, DN; Formal Analysis, software development, and investigation: RC; Writing - original draft: RC, with early feedback on text and figures from JG and BJ; Writing - review and editing: all co-authors

Authors declare no conflict of interest.

[2]correspondence should be addressed to roger.creel@whoi.edu

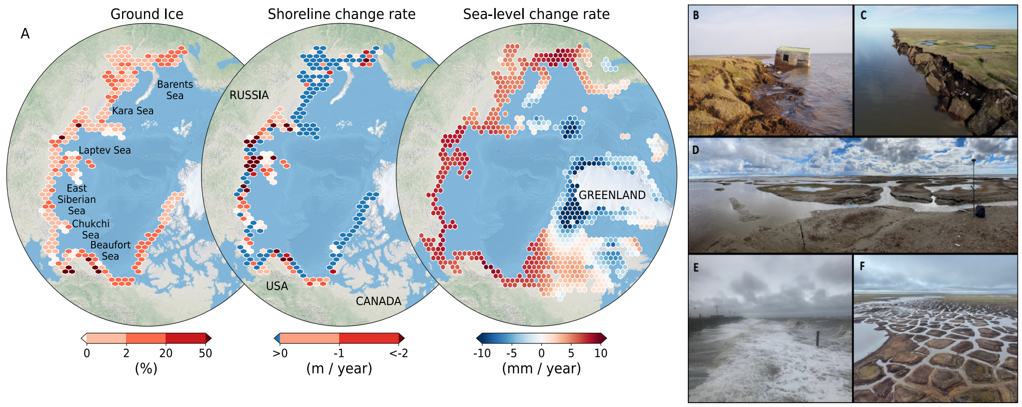

Fig. 1. Variability of Arctic ground ice, shoreline change, and sea level. **(A)** Ground ice and shoreline data are from the ACD database (14). Sea-level change rates (2020-2100 mean) are for the IPCC-AR6's mid-level emissions scenario (SSP2-4.5) (15, 16). **B** Erosion undercuts an Iñupiaq cabin, Elson Lagoon, Alaska. **C** Cabin-sized permafrost blocks collapse into the Beaufort Sea, Drew Point. **D** Seawater drowns ice wedge polygonal tundra, Ikpikpuk Delta, Alaska. **E** Storm threatens infrastructure, Utqiagvik, Alaska. **F** Marine flooding degrades permafrost, Point Lonely, Alaska. Images from coauthor BMJ.

intensifying permafrost coastal dynamics. For instance, along the US Beaufort Sea coast, shoreline change increased 80% from the 1970s to 2000s and 133% from the 2000s to 2010s (2). Coastal erosion has significant impacts on municipal infrastructure and property (8) as well as on natural resource-based land uses (9). For these reasons, efforts to stabilize shorelines often focus on erosion (10).

Permafrost subsidence has also been identified as a coastal threat. Permafrost-related vertical land motion occurs on a range of scales. Seasonal variations in active layer thickness can lead to decimeter-scale cycles of heave and subsidence (11). Fire and human-induced disturbances to tundra environments can also trigger local subsidence rates approaching a decimeter per year, and these rates can persist for decades (12). Human-related disturbances are often associated with built infrastructure, which is one of the landscape types most impacted by Arctic climate evolution: through thermokarst, active layer thickening, mass movement, and other warming-related hazards, permafrost degradation undermines roads, damages pipelines, and destabilizes building foundations (13).

Over broader regions, repeated measurement of permafrost elevations began around the middle of the 20th century to identify centimeter-scale annual subsidence of ice-rich permafrost (17). This land motion has been attributed to late-season melting of ground ice driven by warming near-surface air temperatures (18)—a pattern that has accelerated in the 21st century (19). Such 'isotropic' permafrost thaw has been resolved spatially via interferometric synthetic aperture radar (InSAR) (11, 12), which, when paired with differential GNSS or other in-situ observations, can precisely constrain interannual permafrost subsidence.

Sea-level rise regularly features in Arctic threat assessments as a process that will increase the risks posed by extreme events such as ocean surges (20). The projected impacts of sea-level rise on Arctic shorelines are spatially heterogenous. Regions near areas of ice mass unloading—e.g. Arctic Canada, Greenland, Southeast Alaska, Western Siberia—will undergo net sea-level fall due to glacial isostatic adjustment (15, 16). Arctic communities far from rapid isostatic uplift, however, are routinely identified as being at high risk of sea-level rise-driven flooding (2, see Fig. 1). For a few Alaskan communities, this flooding risk has been paired with estimates of permafrost thaw potential to generate comprehensive inundation projections (21). Sea-level projections have also been paired with ground settlement indices and coastal erosion projections at regional scales to develop coastal hazard indices for the Alaskan North Slope (22). In the larger Arctic coastal hazard community, there is broad consensus that regions undergoing high rates of coastal erosion, permafrost subsidence, and sea-level rise are at greatest risk of climate impacts. However, to date, no study has projected the compounding effect that these processes will have on Arctic shorelines and lowlying tundra landscapes (2, 7).

We address this knowledge gap by producing the first projections of 21st century Arctic shoreline position to account for coastal erosion, permafrost subsidence, and sea-level rise. We focus on Alaska's Arctic Coastal Plain (ACP, Fig. 2), which has an abundance of ice-rich permafrost, a high density of low-lying landforms, and among the highest rates of sea-level rise in the Arctic (15, 16). Constraining ACP shoreline position is uniquely possible because of high data density, including high-resolution topographic maps, numerous observations of permafrost landscape characteristics, and a long history of coastal retreat estimation. We first join a 5-meter ACP digital elevation model with InSAR-derived lake depth estimates (23). We then develop a novel algorithm to erode the ACP following the erosion projections of (24), which based on scenarios defined by the International Panel on Climate Change's AR6 Report. This algorithm includes periodic coastal smoothing to simulate observed coastal erosion dynamics and storm-driven sediment redistribution. Next, we produce novel projections of ACP permafrost subsidence by compiling interannual subsidence measurements from lowlying Arctic regions (Supplementary Fig. S1) and mapping them onto an ACP landform classification dataset (25).

We combine these subsidence and erosion estimates with relative sea-level projections from the Fifth National Climate Assessment (26) to project coastal evolution for the 21st century. With these simulations we quantify land loss due to erosion, permafrost subsidence, and sea-level rise, assess the relative importance of each driver of coastal change over time, and project when land loss due to the combination of inundation and erosion will surpass land loss driven by erosion alone. We then estimate the fraction of present-day ACP infrastructure that the landscape change we project would damage without mitigation measures. Finally, we compute the OC the projected land loss could disturb, where disturb means mobilize through erosion or alter via downward diffusion of seawater into sediment.

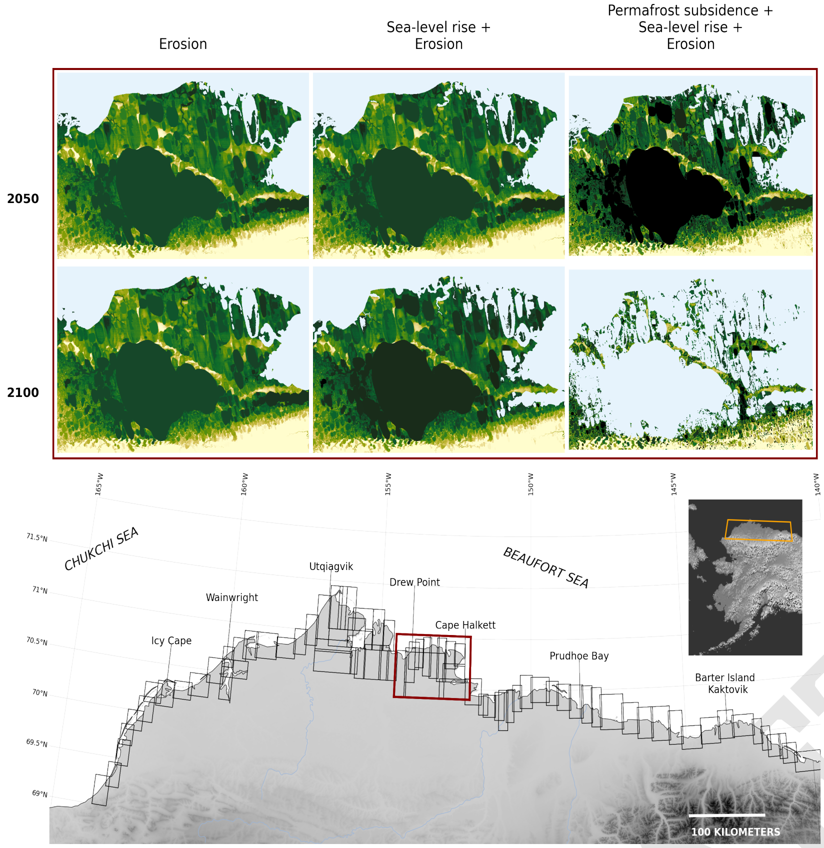

Fig. 2. Evolution of the Teshekpuk Lake region in the 21st century. Black boxes in bottom panel denote Arctic Coastal Plain subregions in which analysis was performed. Inset maps indicate 2050 and 2100 time slices for erosion (left), erosion plus sea-level rise (center), and erosion plus sea-level rise plus permafrost subsidence (right). Colormap denotes topography; light blue is ocean. Projections from a mid-range emissions scenario (SSP2-4.5) are shown.

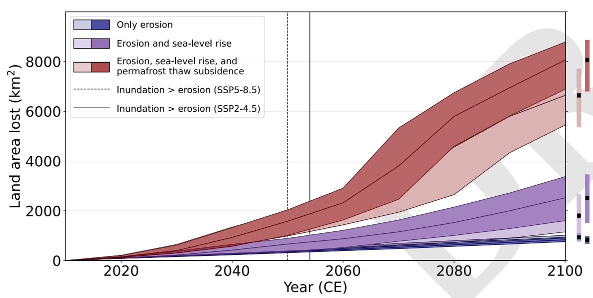

Fig. 3. Projected land loss on Alaska's Arctic Coastal Plain (ACP) over the 21st century. Light/dark blue lines and envelopes (17th to 83rd quantile) represent land loss due to erosion under an medium/high emissions scenario (SSP2-4.5/SSP5-8.5); Purple lines, the combined effect of erosion and sea-level rise; Red lines, the combined effect of erosion, permafrost subsidence, and sea-level rise. Vertical line represents period after which land lost due to the combination of inundation and erosion is virtually certain ($P > 0.99$) to exceed land lost due to erosion alone under medium (solid) and high (dashed) emissions scenarios.

1. Results and Discussion

A. Land loss. We find that under a medium emissions scenario the ACP loses 1469 km^2 (989–1956 km^2, 68% credible interval) of land by 2050 and 6638 km^2 (5446-7620 km^2) by 2100 (Fig. 3)—an area larger than Trinidad and Tobago. With high emissions, those projections increase to 1581 km^2 (1014-2036 km^2) of land by 2050 and 8059 km^2 (6886-8778 km^2) of land by 2100—an area nearly the size of Puerto Rico.

We compare our projections to existing regional tallies of land loss from the combination of erosion and inundation. Merging sediment flux measurements at 48 sites with historical observations, (27) estimated Beaufort Sea land loss is 2.03 km^2/yr. Teshekpuk Lake Special Area, with ∼140 km of shoreline, lost 0.65 km^2/yr from 1979 to 2002, while a ∼40 km length of shoreline from Sagavanirktok River delta to Point Thomson lost 0.76 km^2/yr from 2006 to 2010 (28). These latter rates, scaled to the full ACP shoreline, would equal ∼ 9 and 38 km^2/yr land loss, respectively. Our land loss rates at 2020 fall within these existing rates of ACP land area loss, but under medium or high emissions scenarios will exceed existing rates by mid-century (Fig. 3).

Permafrost subsidence amplifies land loss. Accounting for permafrost subsidence and sea-level rise in addition to erosion leads to mean additional land loss of 4832(5539) km^2 under medium(high) emissions (Fig. 3). The difference between projections that only include erosion vs. those that include both erosion and inundation is stark: including inundation increases land loss six-fold under medium emissions and eight-fold under high emissions. Including inundation also amplifies *rates* of land loss. With only erosion, mean 21st century ACP land loss never exceeds 10.8 km^2/yr. With erosion and sea-level rise, mean land loss rises from 19(22) km^2/yr by 2050 to 33(54) km^2/yr by 2100 under medium(high) emissions. With erosion, sea-level rise, and permafrost subsidence, land loss accelerates to 64 km^2/yr by 2050 in either emissions scenario and peaks at 173(209) km^2/yr by 2072/2076 under medium(high) emissions.

ACP land loss accelerates in the 21st century because linear subsidence increases drive non-linear inundation increases. The ACP is covered with lakes and drained lake basins, the beds of which are typically not more than a few meters above sea level. By mid-century, as permafrost subsidence lowers

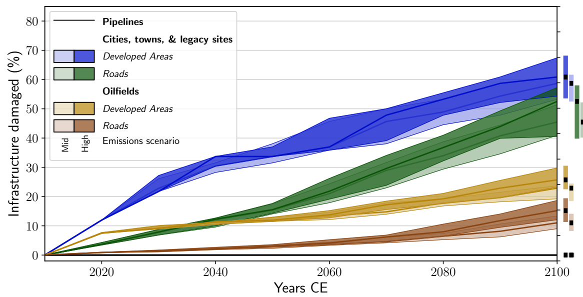

Fig. 4. Present-day infrastructure damaged by coastal change on Alaska's Arctic Coastal Plain (ACP) over the 21st century. Light/darker blue and green lines and envelopes represent developed areas of ACP cities, towns, and legacy sites and related roads damaged by coastal change under medium/high emissions scenarios (SSP2-4.5/SSP5-8.5); brown/yellow lines, the same but for oilfields. Black line denotes oil pipeline damages. Envelopes are 17th to 83rd quantile.

the landscape towards sea level, those lakes connect with the ocean and their margins begin to erode, exposing more lakes to inundation. This fractal behavior can in some settings stabilize shorelines by dampening erosion (29). However, the fractal shoreline behavior modeled here does not depend on erosion: the ∼6000 km^2 more land lost when permafrost subsidence is included occurs with no change in erosion rates, and the difference between medium versus high emissions scenario erosion rates has only a modest impact on that result. Rather, land loss accelerates because of the ACP's >13,000 lakes and drained-lake basins, a low-lying, high-relief system that last flooded between 70 and 115 kyr ago, the last time Earth was substantially warmer than present (30).

B. Impacts to Society. We quantify the fraction of present-day infrastructure that erosion and inundation would damage over the 21st century without mitigation measures. Under medium emissions, erosion and inundation by 2100 damage 59(53-61)% of developed areas and 45(41-51)% of roads in ACP cities, towns, and legacy sites, while in ACP oilfields, 23(19-24)% of developed areas, 11(9-13)% of roads, and 0% of pipelines are damaged. A high emissions scenario increases these projections modestly (Fig. 4). Some infrastructure damage happens before other damage. Developed areas are impacted at highest rates before 2040. Roads connecting cities, towns, and legacy sites are impacted most after 2050, while oilfield-related roads are minimally impacted. These differences reflect the elevational and geographic distributions of each infrastructure type: developed areas tend to occupy low-lying coastal sites (e.g. Prudhoe Bay), while roads span a range of elevational terrains and pipelines stretch directly inland. The largest uncertainty in future infrastructure damages is human action. The damages we project could be amplified if more infrastructure is built in low-lying coastal areas, or lessened if industries and governmental agencies commit to protect or relocate the infrastructure currently under threat. We do not account for this uncertainty in action.

C. Organic carbon impacts. We next quantify the OC that 21st century ACP coastal change could disturb. Erosion-related disturbance includes block failure, thaw slumping, and mechanical abrasion that thaws and mobilizes OC to the marine environment. Inundation-related disturbance includes thawing, seawater intrusion, and mobilization by wave action. We assume that OC is disturbed to a depth of 2 m below sea level in areas that are eroded or inundated, and that disturbed OC stocks are no more than estimated OC stocks in the top 3 m.

We estimate that under medium and high emissions scenarios, erosion and inundation will by 2100 disturb 453 (367-524, 68% credible interval) and 562 (476-616) Tg OC, respectively, which is eight and eleven times the cumulative OC that erosion alone could disturb by 2100 (Supplementary Fig. S2). Mean OC disturbance rates rise from 0.7 Tg C/yr at 2020 to 11(14) Tg C/yr at 2100 under medium(high) emissions. Our 2020 rates exceed, but are of similar magnitude to, previous estimates of present-day OC fluxes from Alaskan Beaufort Sea coastal erosion—0.16 Tg OC/yr (27)—and by 2100 will be ∼40 times the present-day OC fluxes from the three largest rivers draining the ACP (∼0.3 Tg OC/yr) (31). While quantitative conversion of our disturbed OC into greenhouse gas emissions exceeds this paper's scope, if ∼1-10% becomes converted to CO_2, atmospheric CO_2 would rise ∼0.025-0.25 ppm by 2100 (32). Terrestrial OC degradation could further effect the regional marine ecosystem by tipping marginal Arctic seas from sinks to sources of atmospheric CO_2 (e.g. 33), acidifying the ocean (34), altering marine productivity (35), and reshaping Beaufort Sea food webs (36). These impacts highlight the need to consider permafrost subsidence, sea-level rise, and erosion in projections of OC mobilization and transformation.

2. Future Arctic Coasts

Human activity is changing the Earth System fast enough that the recent past has lost predictive power as a template for the future (37). Instead, climate science disciplines are reaching deeper into the past to find analogues for the *states* of future Earth, the *rates* of future change, and the *relative importance* of the processes making that change.

We argue that portions of the Arctic shoreline will undergo transformative changes not only in state and rate—more land lost, increased erosion—but also in which processes drive change. For at least the last century, erosion has governed coastal change everywhere in the Arctic, save locations where glacial isostatic uplift dominates (38, Fig. 1A). We project that for the Beaufort Sea coast this status quo will tip by mid-century as land loss due to the combination of inundation and erosion overtakes land loss due to erosion alone. This transition will likely also occur elsewhere in the Arctic. The shift will happen faster in areas far from ice sheets like the East Siberian, Laptev, and Barents Seas. However, areas with isostatic uplift will not be immune: some parts of Northwest Svalbard have undergone net subsidence for the last century because of permafrost thaw (39). While erosion will continue to dominate in areas with high bluffs, such as the Alaskan Chukchi margin between Wainwright and Utqiaġvik, more and more of the Arctic will enter an inundation paradigm.

The consequences of this paradigm shift are hard to predict but will likely be profound. Little is known about how permafrost evolves when it is inundated versus eroded (40). Rapid inundation may insulate permafrost from increasingly high Arctic summer temperatures that, by season's end, are degrading Pleistocene permafrost—a process that causes landscape-scale subsidence (18). This insulating effect will lessen, however, as mean annual Arctic Ocean bottom temperatures exceed 0°C—which they are projected to do throughout the Arctic by mid-century—and subsea permafrost thaws rapidly from above (41). Inundation could also change the fate of OC by shifting redox conditions: eroded material is likely to degrade faster under aerobic conditions in the water column, whereas inundated material could degrade more slowly under anaerobic conditions in the subsurface. Alternatively, inundation may degrade more permafrost by covering it with salty brine that, as it percolates downwards, will drive thaw by reducing the permafrost melting point (40).

Either way, an Arctic shoreline governed by inundation will pose new challenges to communities whose homelands—including infrastructure, hunting grounds, subsistence access routes, heritage sites, landscapes, and the soil itself—are disappearing. Future research on Arctic shoreline evolution should be motivated by the needs of these communities, who will need support to respond to the paradigm shift in 21st century Arctic coastal change that we project here.

Materials and Methods

Future ACP evolution is projected using a 5 meter Alaska Digital Elevation Model (hereafter, DEM) based on InSAR source data of 5-meter or higher resolution collected between 2012 and 2018 (42). We take 2015 as our simulation's first year. The DEM is split into 78 overlapping subregions $S \in DEM$ that encompass all coastal areas that in our maximum projections are inundated or eroded by 2100 (Fig. 2). Computations described below are performed on each subregion in isolation. Overlapping sections are then compared, and any pixel covered by ocean in either section is considered to be land replaced by ocean—a procedure that prevents double-counting.

Topography is defined as positive relief (H) in DEM areas above mean sea level in 2015:

$$H(x, y) = DEM(x, y) \cdot C(x, y), \quad [1]$$

where the ocean function $C(x, y)$ is defined by

$$C(x, y) = \begin{cases} 1 & \text{if } DEM(x, y) > 0 \\ \varnothing & \text{if } DEM(x, y) \leq 0 \end{cases} \quad [2]$$

We note that (1) led to all terrestrial and lacustrine areas being correctly identified as land.

Lake depth correction. The DEM represents freshwater lakes as flat areas whose elevation equals the unfrozen surface water elevation. To approximate lake bathymetry in these flat areas, we follow (23) (https://catalog.northslopescience.org/hr/dataset/2285), who found that North Slope lakes that froze completely in winter were 94% likely to be shallower than 1.6 m, while lakes that remained at least partly unfrozen were 98% likely to be more than 1.6 m deep. We derive an initial topography (T) by correcting elevation (H) for the depth of these lakes (L):

$$T_0(x, y) = H_0(x, y) - L(x, y), \quad [3]$$

where lake depth $L(x, y)$ is defined by

$$L(x, y) = \begin{cases} 2.0 \; meters & \text{if not frozen solid in winter} \\ 1.0 \; meter & \text{if frozen solid in winter} \end{cases} \quad [4]$$

Lake depths were derived from the median empirical frozen and unfrozen lake depth distributions from (23). Because median lake depth exceeds 2 m, this correction likely leads us to underestimate lake depth overall and is therefore a conservative choice.

Sea-level change. Relative sea level (RSL) change is estimated following projections from the 5th National Climate Assessment (NCA5 26). These projections account for RSL change due to several processes, including thermal expansion, the melting of mountain glaciers and the Greenland and Antarctic ice sheets, and vertical land motion (VLM), which encompasses regional processes like glacial isostatic adjustment (GIA, the gravitational, deformational, and rotational response of the solid Earth to changes in ice and liquid water loading (43)) and local processes like groundwater pumping. The NCA5 assesses VLM via a statistical model that converts tide-gauge observations into a spatially varying but temporally linear RSL change rate (15, 16). This assessment's accuracy depends on tide gauge density. Long-term, high-quality tide gauge records are scarce in northern Alaska: the Permanent Service on Mean Sea Level includes only a single ACP gauge (Prudhoe Bay). The NCA5 projections' 1-degree gridding also implies that processes driving nearshore VLM resemble those driving VLM on land. This assumption breaks down when interannual VLM is dominated by permafrost subsidence. Additionally, the Prudhoe Bay gauge cannot capture the spatial variability in ACP permafrost subsidence. For these reasons, it is unlikely the NCA5 RSL projections accurately represent present-day ACP VLM rates from permafrost subsidence. We therefore model that VLM component separately.

Permafrost subsidence. We estimate permafrost subsidence using an empirical approach. We aggregate interannual permafrost subsidence estimates from low-lying regions in Alaska, Arctic Canada, and Russia (See Supplemental Fig. S1). To be included, a record must meet several criteria. First, it must span 3+ years. Second, records must be based off high-precision measurement, for instance differential GNSS measurements repeated at the same time each year (19), differential GNSS combined with InSAR, thaw tube measurements, or repeat terrestrial laser scanning (rLiDAR) benchmarked by GNSS (11, 12, 17). Subsidence from GNSS—though not from InSAR, thaw tube, or other relative measurements—contains glacial isostatic adjustment, which the NCA5 sea-level estimates also include. However, this duplication is not an issue, as ACP GIA (0.1-0.3 mm/year, (44)) is much smaller than permafrost subsidence uncertainties (Supplemental Fig. S1). Third, records must describe the landscape type whose subsidence is measured. We map subsidence estimates onto Landsat-derived ACP landscape classifications (25). Landscape type correlates strongly with ground ice content (45) and late-season thawing of sub-active layer ground ice (18). Since late-season ground ice thaw likely drives interannual landscape-scale permafrost subsidence (19)—and no sub-kilometer-scale ACP ground ice estimates exist—we use landscape type as a proxy for permafrost subsidence.

Erosion. Erosion (E) is estimated for each subregion following spatially-varying projections from a semi-empirical model that combines climate reanalyses, observations, Earth system modeling, and ocean surface wave simulations (24). Erosion is initialized as 0 at 2015. For each subsequent year, the mean erosion projected by (24) for each subregion is added to the previous year's erosional tally:

$$E_t = E_{t-1} + \frac{\sum_{x=1}^{n} \sum_{y=1}^{m} E_t(x, y)}{n \cdot m} \quad [5]$$

where n and m are subregion dimensions. When E_t exceeds 5, a threshold set by the 5 m DEM resolution, erosion initiates. Erosion is simulated by convolving a 3x3 cross-shaped kernel (K_e) across the subregion. Eroding regions—non-ocean areas with sum >50% of the kernel sum, a threshold that isolates shorelines regardless of orientation—are reclassified as ocean:

$$S_e(x, y) = \begin{cases} S(x, y) & \text{where } S(x, y) * K_e < \frac{1}{2} \sum K_e \\ \varnothing & \text{where } S(x, y) * K_e > \frac{1}{2} \sum K_e \end{cases} \quad [6]$$

where S_e is a post-erosion subregion. Erosion here resembles the erosional operator in mathematical morphology, a standard image processing tool.

By implementing (24), our erosion algorithm accounts for the main thermo-mechanical drivers of 21st century erosion, namely temperature, sea ice and ocean surface waves. However, it does not explicitly resolve coastal erosion itself. Rather, it relies on empirical relationships between erosion and its thermo-mechanical drivers. Physics-based, explicit models of coastal permafrost erosion first modeled niche evolution as an analytical function of ocean temperature, nearshore water depth, and inundation duration, then successively reproducing niche growth, bluff failure, slumping, wave propagation, thermodenudation, thermal abrasion, sediment transport, and other processes to project lateral cliff migration and vertical erosion of abutting beaches (46). These models are routinely applied to 1D shoreline transects, but never expanded to 3D to project erosion at regional or climatic scales (47) due to impractical computational costs. We therefore employ this simpler algorithm as an approximation, which allows us to assess the relative importance of erosion, permafrost subsidence, and sea-level rise at regional and climatic scales.

Storm smoothing. Storms periodically reshape ACP shorelines. We approximate this process via a procedure similar to Equation 6. We convolve a 10x10 boxcar kernel (K_s) across each subregion. Terrestrial coastal areas whose convolved sum is $< 50\%$ the sum of K_s are reclassified as ocean. Coastal ocean areas whose convolved sum exceeds half the sum of K_s are reclassified as land with 1 meter topographic relief:

$$S_s(x,y) = \begin{cases} \varnothing & \text{where} S_e(x,y) * K_s < \frac{1}{2}\sum K_s \\ 1 & \text{where } S_e(x,y) * K_s > \frac{1}{2}\sum K_s \end{cases} \qquad [7]$$

This operation redistributes sediment along the coast with a smoothing lengthscale of 50 meters. Modest changes in K_s size were found to have negligible impact on our results.

Inundation. Inundation converts coastal ACP regions at sea level into marine inlets. We model this by convolving a 10x10 circular kernel across each subregion to identify areas within 50 m of the coast. Areas <0.2 m above sea level in this zone—a threshold set by ACP tidal amplitudes—are reclassified as ocean. This protocol elides short-term nearshore processes that could dampen local post-inundation erosion rates. However, on decadal timescales, erosional breaching of freshwater lakes, inundation, and subsequent erosion of former lake shorelines has been observed across the ACP (28). We therefore argue that immediate inundation is a reasonable approximation.

Infrastructure. The fraction of infrastructure damaged by erosion and inundation is estimated using the infrastructure maps of the North Slope Science Initiative. We differentiate these maps into 'Developed Areas' and 'Roads' for cities, towns, and legacy sites—i.e. Distant Early Warning Line sites— and oilfields as well as oil pipelines. We consider developed area polygons damaged if they intersect with the ocean. Road polygons are damaged only at the specific locations where seawater covers them.

Organic carbon. We quantify the OC disturbed by erosion and inundation by employing a 300 m circumpolar soil carbon dataset (48). Topography in subregion S at each timestep is compared to 2015 topography. OC is deemed disturbed at time t if the area is ocean at time t but had topography in 2015. OC disturbance is quantified by (48) in only the top 3 m of sediment, and we assume that all deeper sediment contains no OC. This choice likely leads us to underestimate OC disturbance, particularly in areas with high coastal relief.

Inundation is modeled as disturbing OC down to 2 m below sea level. Three factors determined this depth: tidal range, estimated as 10-20 cm; active layer thickness of inundated sediments, estimated as 30-40 cm; and historical patterns of nearshore erosion and deposition. From comparisons between 1945-1953 and 2012-2015 hydrographic surveys, (49) describes 0.5 to 3+ meters of erosion beyond barrier islands and 0 to 0.5 meters of deposition within lagoon systems. In future, heightened 21$^{\text{st}}$ century storminess may increase lagoonal sediment disruption (50). Assuming 21$^{\text{st}}$ century sediment disruption depths fall in the mid-range of historical ranges, 2 meters of disruptive penetration by erosion is a conservative choice, particularly given this study's biogeochemical focus on OC disruption, which here encompasses sediment redistribution as well as erosion. Furthermore, even where erosion disturbs little, inundation causes rapid changes in the shallow subsurface. For instance, hypersaline brines produced during sea-ice formation percolate through newly-inundated permafrost, lowering sediment freezing temperatures and accelerating thaw even with <2 meters of inundation (51). Sediment resuspension, temperature, redox conditions, organic matter quality, and other factors impact the rate in which disturbed OC is remineralized. Given these uncertainties, we use a few simple assumptions: 2 m bsl of OC is disturbed, and 1-10% of disturbed OC is remineralized to CO_2-C (32).

ACKNOWLEDGMENTS. We thank Chris Piecuch and Christina Schädel for helpful discussions that improved this manuscript and the Permafrost Coastal Systems Network (PerCS-Net) for building the connections that sparked this work. Funding for this research was provided by a Woods Hole Oceanographic Institution Postdoctoral Scholarship (RC) and several grants from the U.S. National Science Foundation (OISE-1927553, OISE-1927373, OPP-1836861, OPP-2322664, OPP-1903735, RISE-2318375, OPP-2336165).

1. M Rantanen, et al., The Arctic has warmed nearly four times faster than the globe since 1979. *Commun. Earth & Environ.* **3**, 1–10 (2022) Publisher: Nature Publishing Group.
2. AM Irrgang, et al., Drivers, dynamics and impacts of changing Arctic coasts. *Nat. Rev. Earth & Environ.* **3**, 39–54 (2022) Publisher: Nature Publishing Group.
3. RM Buzard, et al., Current and projected flood exposure for Alaska coastal communities. *Sci. Reports* **14**, 7765 (2024).
4. JE Overland, M Wang, JE Walsh, JC Stroeve, Future Arctic climate changes: Adaptation and mitigation time scales. *Earth's Futur.* **2**, 68–74 (2014) _eprint: https://agupubs.onlinelibrary.wiley.com/doi/pdf/10.1002/2013EF000162.
5. J Overbeck, R Buzard, M Turner, K Miller, R Glenn, Shoreline change at Alaska coastal communities, (Alaska Division of Geological & Geophysical Surveys), Technical Report RI 2020-10 (2020).
6. EC Cabot, The Northern Alaskan Coastal Plain Interpreted from Aerial Photographs. *Geogr. Rev.* **37**, 639–648 (1947) Publisher: [American Geographical Society, Wiley].
7. BM Jones, et al., Arctic Report Card 2020: Coastal Permafrost Erosion. *NOAA Arct. Rep. Card* (2020) Publisher: [object Object].
8. RM Buzard, et al., Barrier Island Reconfiguration Leads to Rapid Erosion and Relocation of a Rural Alaska Community. *J. Coast. Res.* **39**, 625–642 (2023).
9. MB Brady, R Leichenko, The impacts of coastal erosion on Alaska's North Slope communities: a co-production assessment of land use damages and risks. *Polar Geogr.* **43**, 259–279 (2020) Publisher: Taylor & Francis _eprint: https://doi.org/10.1080/1088937X.2020.1755907.
10. M Liew, M Xiao, BM Jones, LM Farquharson, VE Romanovsky, Prevention and control measures for coastal erosion in northern high-latitude communities: a systematic review based on Alaskan case studies. *Environ. Res. Lett.* **15**, 093002 (2020) Publisher: IOP Publishing.
11. L Liu, T Zhang, J Wahr, InSAR measurements of surface deformation over permafrost on the North Slope of Alaska. *J. Geophys. Res. Earth Surf.* **115** (2010) _eprint: https://onlinelibrary.wiley.com/doi/pdf/10.1029/2009JF001547.
12. L Liu, et al., Remote sensing measurements of thermokarst subsidence using InSAR. *J. Geophys. Res. Earth Surf.* **120**, 1935–1948 (2015) _eprint: https://onlinelibrary.wiley.com/doi/pdf/10.1002/2015JF003599.

13. J Hjort, et al., Impacts of permafrost degradation on infrastructure. *Nat. Rev. Earth & Environ.* **3**, 24–38 (2022) Number: 1 Publisher: Nature Publishing Group.
14. H Lantuit, PP Overduin, S Wetterich, Recent Progress Regarding Permafrost Coasts. *Permafr. Periglac. Process.* **24**, 120–130 (2013) _eprint: https://onlinelibrary.wiley.com/doi/pdf/10.1002/ppp.1777.
15. GG Garner, et al., IPCC AR6 Sea Level Projections (2021).
16. Fox-Kemper, B., et al., 2021: Ocean, cryosphere and sea level change. *The Sixth Assess. Rep. Intergov. Panel on Clim. Chang.* (2021).
17. HB O'Neill, SL Smith, CR Burn, C Duchesne, Y Zhang, Widespread Permafrost Degradation and Thaw Subsidence in Northwest Canada. *J. Geophys. Res. Earth Surf.* **128**, e2023JF007262 (2023) _eprint: https://agupubs.onlinelibrary.wiley.com/doi/pdf/10.1029/2023JF007262.
18. S Zwieback, FJ Meyer, Top-of-permafrost ground ice indicated by remotely sensed late-season subsidence. *The Cryosphere* **15**, 2041–2055 (2021) Publisher: Copernicus GmbH.
19. NI Shiklomanov, DA Streletskiy, JD Little, FE Nelson, Isotropic thaw subsidence in undisturbed permafrost landscapes. *Geophys. Res. Lett.* **40**, 6356–6361 (2013) _eprint: https://onlinelibrary.wiley.com/doi/pdf/10.1002/2013GL058295.
20. AK Magnan, et al., Sea level rise risks and societal adaptation benefits in low-lying coastal areas. *Sci. Reports* **12**, 10677 (2022) Publisher: Nature Publishing Group.
21. TC Lantz, ND Moffat, BM Jones, Q Chen, CE Tweedie, Mapping Exposure to Flooding in Three Coastal Communities on the North Slope of Alaska Using Airborne LiDAR. *Coast. Manag.* **48**, 96–117 (2020) Publisher: Taylor & Francis _eprint: https://doi.org/10.1080/08920753.2020.1732798.
22. Z Wang, et al., Arctic coastal hazard assessment considering permafrost thaw subsidence, coastal erosion, and flooding. *Environ. Res. Lett.* **18**, 104003 (2023) Publisher: IOP Publishing.
23. J Grunblatt, D Atwood, Mapping lakes for winter liquid water availability using SAR on the North Slope of Alaska. *Int. J. Appl. Earth Obs. Geoinformation* **27**, 63–69 (2014).
24. DM Nielsen, et al., Increase in Arctic coastal erosion and its sensitivity to warming in the twenty-first century. *Nat. Clim. Chang.* **12**, 263–270 (2022) Number: 3 Publisher: Nature Publishing Group.
25. M Lara, I Nitze, G Grosse, A McGuire, Tundra landform and vegetation productivity trend maps for the Arctic Coastal Plain of northern Alaska. *Sci. Data* **5**, 180058 (2018).
26. WV Sweet, et al., Interagency report: Global and Regional Sea Level Rise Scenarios for the United States: Updated Mean Projections and Extreme Water Level Probabilities Along U.S. Coastlines (2022).
27. CL Ping, et al., Soil carbon and material fluxes across the eroding Alaska Beaufort Sea coastline. *J. Geophys. Res. Biogeosciences* **116** (2011) _eprint: https://agupubs.onlinelibrary.wiley.com/doi/pdf/10.1029/2010JG001588.
28. BM Jones, et al., Increase in the rate and uniformity of coastline erosion in Arctic Alaska. *Geophys. Res. Lett.* **36** (2009).
29. B Sapoval, A Baldassarri, A Gabrielli, Self-Stabilized Fractality of Seacoasts through Damped Erosion. *Phys. Rev. Lett.* **93**, 098501 (2004) Publisher: American Physical Society.
30. LM Farquharson, et al., Climate Change Drives Widespread and Rapid Thermokarst Development in Very Cold Permafrost in the Canadian High Arctic. *Geophys. Res. Lett.* **46**, 6681–6689 (2019) _eprint: https://agupubs.onlinelibrary.wiley.com/doi/pdf/10.1029/2019GL082187.
31. JW McClelland, et al., River export of nutrients and organic matter from the North Slope of Alaska to the Beaufort Sea. *Water Resour. Res.* **50**, 1823–1839 (2014).
32. B Wild, et al., Organic matter composition and greenhouse gas production of thawing subsea permafrost in the Laptev Sea. *Nat. Commun.* **13**, 5057 (2022) Publisher: Nature Publishing Group.
33. C Bertin, et al., Biogeochemical River Runoff Drives Intense Coastal Arctic Ocean CO2 Outgassing. *Geophys. Res. Lett.* **50**, e2022GL102377 (2023) _eprint: https://onlinelibrary.wiley.com/doi/pdf/10.1029/2022GL102377.
34. I Semiletov, et al., Acidification of East Siberian Arctic Shelf waters through addition of freshwater and terrestrial carbon. *Nat. Geosci.* **9**, 361–365 (2016) Publisher: Nature Publishing Group.
35. J Terhaar, O Torres, T Bourgeois, L Kwiatkowski, Arctic Ocean acidification over the 21st century co-driven by anthropogenic carbon increases and freshening in the CMIP6 model ensemble. *Biogeosciences* **18**, 2221–2240 (2021) Publisher: Copernicus GmbH.
36. KH Dunton, SV Schonberg, LW Cooper, Food Web Structure of the Alaskan Nearshore Shelf and Estuarine Lagoons of the Beaufort Sea. *Estuaries Coasts* **35**, 416–435 (2012).
37. J Knight, S Harrison, Limitations of uniformitarianism in the Anthropocene. *Anthropocene* **5**, 71–75 (2014).
38. H Lantuit, et al., The Arctic Coastal Dynamics Database: A New Classification Scheme and Statistics on Arctic Permafrost Coastlines. *Estuaries Coasts* **35**, 383–400 (2012).
39. M Rolf, I Grünberg, J Hammar, J Boike, Quantifying thaw subsidence in a permafrost landscape (Bayelva basin, Svalbard), (Copernicus Meetings), Technical Report EGU24-7901 (2024).
40. N Shakhova, et al., Current rates and mechanisms of subsea permafrost degradation in the East Siberian Arctic Shelf. *Nat. Commun.* **8**, 15872 (2017).
41. RC Creel, F Miesner, S Wilkenskjeld, J Austermann, PP Overduin, Glacial isostatic adjustment reduces past and future Arctic subsea permafrost. *Nat. Commun.* **15**, 3232 (2024) Publisher: Nature Publishing Group.
42. UG Survey, The National Map—New data delivery homepage, advanced viewer, lidar visualization, US. Geological Survey Fact Sheet 2019–3032 (2019).
43. WE Farrell, JA Clark, On Postglacial Sea Level. *Geophys. J. Royal Astron. Soc.* **46**, 647–667 (1976).
44. CA Ludwigsen, SA Khan, OB Andersen, B Marzeion, Vertical Land Motion From Present-Day Deglaciation in the Wider Arctic. *Geophys. Res. Lett.* **47**, e2020GL088144 (2020) _eprint: https://onlinelibrary.wiley.com/doi/pdf/10.1029/2020GL088144.
45. M Kanevskiy, et al., Ground ice in the upper permafrost of the Beaufort Sea coast of Alaska. *Cold Reg. Sci. Technol.* **85**, 56–70 (2013).
46. N Kobayashi, Numerical Modeling of Wave Runup on Coastal Structures and Beaches. *Mar. Technol. Soc. J.* **33**, 33–37 (1999).
47. R Rolph, PP Overduin, T Ravens, H Lantuit, M Langer, ArcticBeach v1.0: A physics-based parameterization of pan-Arctic coastline erosion. *Front. Earth Sci.* **10** (2022) Publisher: Frontiers.
48. J Palmtag, et al., A high spatial resolution soil carbon and nitrogen dataset for the northern permafrost region based on circumpolar land cover upscaling. *Earth Syst. Sci. Data* **14**, 4095–4110 (2022) Publisher: Copernicus GmbH.
49. M Zimmermann, et al., Nearshore bathymetric changes along the Alaska Beaufort Sea coast and possible physical drivers. *Cont. Shelf Res.* **242**, 104745 (2022).
50. LH Erikson, et al., Changing storm conditions in response to projected 21st century climate change and the potential impact on an arctic barrier island–lagoon system—A pilot study for Arey Island and Lagoon, eastern Arctic Alaska, (U.S. Geological Survey), Technical Report 2020-1142 (2020).
51. V Rachold, et al., Nearshore arctic subsea permafrost in transition. *Eos, Transactions Am. Geophys. Union* **88**, 149–150 (2007) _eprint: https://onlinelibrary.wiley.com/doi/pdf/10.1029/2007EO130001.

Supporting Information for

Permafrost thaw subsidence, sea-level rise, and erosion are transforming Alaska's Arctic coastal zone

Roger Creel, Julia Guimond, Benjamin Jones, David M. Nielsen, Emily Bristol, Craig Tweedie, Pier Paul Overduin

Roger Creel
E-mail: roger.creel@whoi.edu

This PDF file includes:

Figs. S1 to S2
SI References

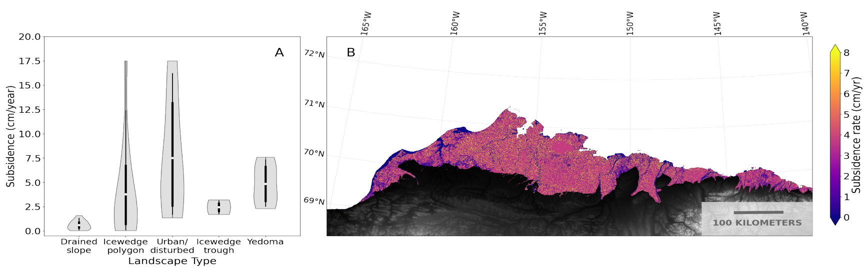

Fig. S1. Permafrost subsidence on Alaska's Arctic Coastal Plain (ACP) **(A)** Empirical estimates of permafrost subsidence from coastal Arctic landscapes. White dots denote means, vertical lines mark 66% and 95% confidence intervals. **(B)** Modeled permafrost subsidence based on mapping of empirical estimates to landscape classifications from (1).

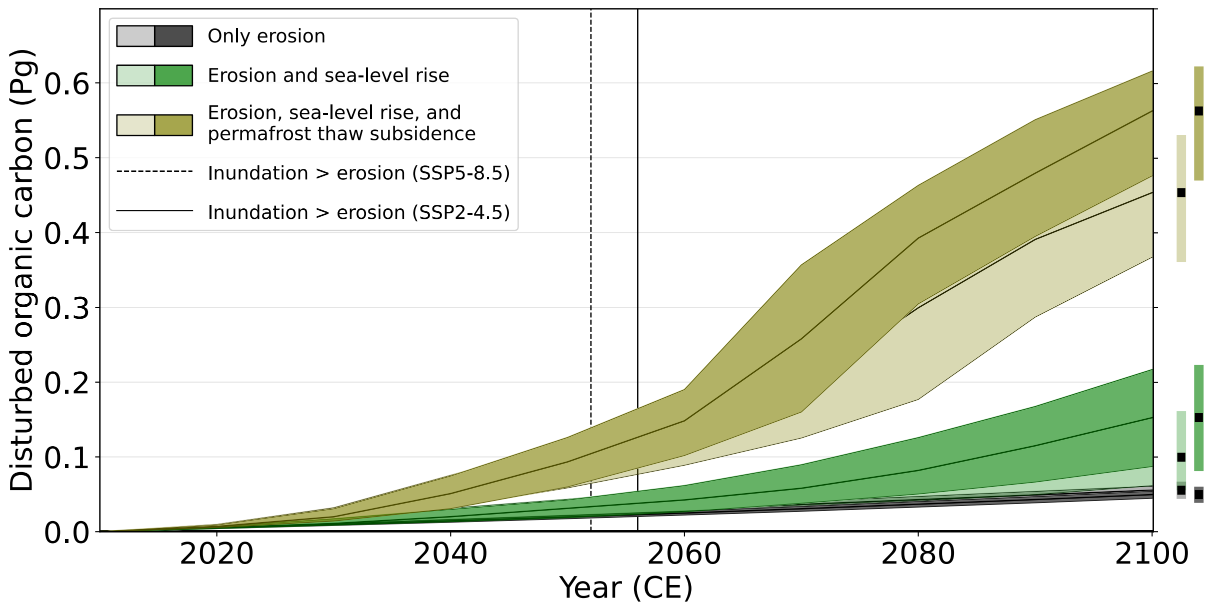

Fig. S2. Organic carbon disturbed by coastal change on Alaska's Arctic Coastal Plain (ACP) over the 21st century. Light/dark grey lines and envelopes represent organic carbon (OC) disturbed due only to erosion under an medium/high emissions scenario (SSP2-4.5/SSP5-8.5); emerald-green lines, OC disturbed due to the combined effect of erosion and sea-level rise; olive lines, due to the combined effect of erosion, permafrost subsidence, and sea-level rise. Envelopes are 17th to 83rd quantile. Grey area represents time period after which inundation is virtually certain ($P >$0.99) to exceed erosion as the dominant agent of OC disturbance under medium (solid vertical line) and high (dashed vertical line) emissions scenarios.

References

1. M Lara, I Nitze, G Grosse, A McGuire, Tundra landform and vegetation productivity trend maps for the Arctic Coastal Plain of northern Alaska. *Sci. Data* **5**, 180058 (2018).